J. Plasma Physics (2005), *vol.* 71, *part* 4, *pp.* 411–433.
doi:10.1017/S0022377804003320 Printed in the United Kingdom

On the effect of laser and plasma parameters on stimulated Raman scattering and fast-electron generation

R. M. G. M. TRINES,[1] L. P. J. KAMP,[1] T. J. SCHEP,[1]
F. W. SLUIJTER,[1] W. P. LEEMANS[2] and E. H. ESAREY[2]

[1]Department of Applied Physics, Eindhoven University of Technology, PO Box 513, NL-5600 MB Eindhoven, The Netherlands
(l.p.j.kamp@tue.nl)

[2]Lawrence Berkeley National Laboratory, Berkeley, CA 94720, USA

(Received 28 June 2004 and accepted 30 July 2004)

Abstract. The effect of Raman instabilities on the production of fast electrons in laser–plasma interaction has been investigated for laser intensities well above the electron trapping threshold. The results of one-dimensional particle-in-cell simulations show that in this regime the presence of Raman backscattering (RBS) hampers fast-electron production, and that its suppression increases the yield of high-energy electrons (>15 MeV). Such suppression has been realized either through deletion of all backscattered radiation from the simulations or through direct stimulation of Raman forward scattering (RFS). An increased high-energy electron yield has been observed for both methods. In addition, the influence of various laser and plasma parameters on the production of highly energetic electrons has been investigated. Specifically, the effects of plasma density ramps, skews in the temporal envelopes of the laser pulses, and laser frequency chirp (both pulse-length preserving and bandwidth preserving) have been examined. For each parameter, its influence on the yield of high-energy electrons can be explained from the way it affects the balance between RBS and RFS excitation in laser–plasma interaction.

1. Introduction

Several recent experiments [1–7] on the interaction of intense laser pulses with underdense plasmas have demonstrated the production of energetic electrons in the self-modulated regime of the laser wakefield accelerator (LWFA) [8] with accelerating gradients in excess of $100\,\mathrm{GeV\,m^{-1}}$. The resulting electron bunches are characterized by high charge (up to 10 nC), sub-picosecond duration, and an exponential energy distribution with a mean energy of tens of MeV. Applications of these bunches include injectors to secondary accelerators [9], short-pulse radiation sources [10], short-lived radio-isotope production [11], and fast ignition fusion [12].

In this paper, we investigate the role of Raman backscattering (RBS) in high-energy electron production and the interplay between RBS and Raman forward-scattering (RFS) in the high-intensity regime of a self-modulated LWFA [13]. In previous work [5, 14–19], it has been demonstrated that the presence of RBS leads to the production of mildly energetic electrons. Since these electrons are easily

trapped and accelerated by the laser wake, it has been argued that their presence, and therefore the presence of RBS, improves the yield of high-energy electrons. This has been confirmed for laser intensities slightly above the threshold for plasma electron trapping. In contrast to this, we show that for laser intensities well above the trapping threshold, the converse is true: the presence of RBS can be detrimental to high-energy electron production. It will be demonstrated that for high laser intensities the level of RBS-induced electron trapping increases to the extent that the laser wake is severely damped. This decreases the number of electrons that are accelerated to truly high energies (over 15 MeV), even though the yield of mildly energetic (up to 3 MeV) electrons increases. Consequently, suppressing RBS in the high-intensity regime results in a larger plasma wake and a larger yield of highly energetic electrons. Suppression of RBS has been achieved either by periodically removing all backward-going electromagnetic (EM) waves from the simulation, or by stimulating the growth of RFS. We propose and demonstrate, via one-dimensional particle-in-cell (PIC) simulations, an experimentally realizable RBS suppression method that uses stimulated growth of RFS by seeding the RFS Stokes wave. This results in a higher level of RFS, a larger fast wake, a lower level of RBS, and a larger amount of high-energy electrons.

In addition we investigate the way in which various laser and plasma parameters, such as plasma density profile, pulse envelope shape and laser frequency chirp, influence the production of energetic electrons. From our simulation results, it will be shown that the effect of each parameter on fast-electron yield can be explained from the way it influences the balance between RBS and RFS excitation in laser–plasma interaction. Any parameter that favours RFS growth and/or suppresses RBS growth will also increase the yield of high-energy electrons. Conversely, a parameter that enhances RBS growth and/or hampers RFS growth will decrease the production of highly energetic electrons. This allows us to predict or explain the effect of a number of laser and plasma parameters on high-energy electron yield.

2. Effect of Raman scattering on electron yield

According to basic Raman scattering theory [20–23], RBS is a three-wave interaction, in which the incoming laser light (carrier frequency ω_0, wave number k_0, peak amplitude $E_0 = (m_e\omega_0 c/e)a_0$) decays into a backscattered EM wave $(\omega_0 - \omega_p, -(k_0 - k_p))$ and a slow Langmuir wave $(\omega_p, 2k_0 - k_p)$. Here, $\omega_p = \sqrt{n_0 e^2/(\varepsilon_0 m_e)}$, $k_p = \omega_p/c$, and n_0 is the unperturbed plasma electron density. The Langmuir wave phase velocity is approximately $\omega_p c/(2\omega_0) \ll c$ for an underdense plasma. RBS is characterized by a large growth rate. RFS on the other hand has a much smaller growth rate and involves four waves: the laser light decays in two forward-scattered EM waves, a Stokes wave $(\omega_0 - \omega_p, k_0 - k_p)$ and an anti-Stokes wave $(\omega_0 + \omega_p, k_0 + k_p)$, and a fast Langmuir wave (ω_p, k_p) with phase velocity $\sim c$ provided that $\omega_p \ll \omega_0$. Because of its high phase velocity, the RFS Langmuir wave is well suited for accelerating trapped electrons to high energy [24]. At sufficiently high laser intensities, the breaking of this wave contributes heavily to the trapping and acceleration to high energies of background plasma electrons [3, 24–26]. The RBS Langmuir wave has a much lower wave-breaking amplitude because of its low phase velocity, and thus requires a much lower laser intensity to break. Also, its high growth rate ensures that it is repeatedly pushed to breaking conditions. The

https://doi.org/10.1017/S0022377804003320 Published online by Cambridge University Press

breaking of this wave only yields low-energy electrons (up to several 100 keV). When injected into the RFS Langmuir wave, part of these electrons may be accelerated to higher energies through an RBS–RFS two-stage acceleration mechanism [5, 14–19]. This leads to an improved yield of energetic electrons at lower laser intensities and a decrease of the intensity threshold for electron trapping.

When the laser intensity is increased well beyond the trapping threshold, the following phenomena occur: (i) the laser intensity is such that the plasma wake (i.e. the fast RFS plasma wave) itself starts to break, resulting in large-scale particle trapping even in the case where RBS is absent; (ii) RFS growth is sufficiently large to cause RBS and RFS to overlap in space and time even for femtosecond pulses; and (iii) RBS growth is sufficiently large to cause excessive amounts of plasma electrons to be trapped by the wake. Once trapped, these electrons will cause moderate to heavy beam loading and damping of the wake. Note that if RBS and RFS do not overlap, electron injection into the laser wake can only occur through a multi-stage acceleration mechanism involving backscatter, sidescatter, near-forward and forward scatter [16, 17, 27]. In a one-dimensional setting, sidescatter and near-forward scatter are absent, and wake damping as a result of massive electron injection can only be observed if RBS and RFS overlap in space and time. For this reason, we have made sure that such an overlap does occur in the regime under investigation. The ultimate effect of wake damping on high-energy electron production is a marked decrease in the number of electrons that get accelerated to truly high energies, even though the total number of trapped electrons increases. This leads us to the speculation that the yield of high-energy particles in laser–plasma interaction can be improved if we can somehow suppress the increase in RBS that comes with an increased pump pulse intensity.

We achieve such suppression using two different methods. The first is a purely numerical method in which all backward-going radiation is removed periodically from the simulation during a limited period while leaving the forward-going radiation untouched. This method has specifically been employed to isolate the effect of RBS on high-energy electron production. The second is RFS seeding of the pulse, which has been inspired by the notion that stimulation of RFS growth leads to a decrease in RBS through the mode coupling between the RBS and RFS Langmuir waves [28, 29]. In addition, such stimulation will lead to a larger amplitude laser wake that will be less influenced by RBS-induced beam loading.

An experimentally realizable method for RFS stimulation consists of adding a 'Stokes satellite' to the main laser pulse [30], i.e. a laser pulse having the same duration and a similar envelope as the main pulse, but at the Stokes frequency $\omega_0 - \omega_p$, and peak amplitude of several per cent of the peak amplitude of the laser EM field. The initial level of plasma wake excited by this method is similar to that of beat-wave excitation [24]. However, now the level of the Stokes wave is greatly below that of the pump and the laser–plasma interaction is dominated by RFS. This has the advantage over beat-wave excitation that the accuracy requirements on the pump, seed and plasma frequencies are less stringent. Also, a small level of Stokes laser seeding is easier to realize experimentally than a pulse with two spectral lines of equal intensity. As we show below, the amount of RBS found in our simulations decreases with increasing satellite amplitude.

Everett et al. [28, 29] have presented numerical and experimental results on how a fast phase velocity plasma wave can suppress a slow plasma wave, as well as a theoretical explanation in which the amplitudes of the waves are assumed to

be slowly varying compared with the plasma period. In the linear regime, the amplitude $\delta n_s/n_0$ of the normalized density perturbation of the slow (e.g. RBS) plasma wave is reduced by the factor $1-(\delta n_f/n_0)^2(\omega_0/\omega_p)^2$, where $\delta n_f/n_0$ is the normalized density perturbation associated with the fast (e.g. RFS) plasma wave. This predicts suppression of the RBS wave when $\delta n_f/n_0 \simeq \omega_p/\omega_0$. In seeded RFS, the initial amplitude of the RFS plasma wave is given approximately by beat-wave theory [24], which in the linear regime gives $\delta n_f/n_0 \simeq a_0 a_1 \omega_p \tau/4$, where $c\tau = ct-x$ is the distance behind the head of the laser pulses, and a_0, a_1 are the scaled peak amplitudes of the pump and seed pulse, respectively. This predicts RBS suppression for $a_0 a_1 \simeq 4/(\omega_0\tau)$. If RBS is to be suppressed within a single plasma period, i.e. $c\tau = \lambda_p$, this requires a wave amplitude product of $a_0 a_1 \simeq (2/\pi)(\omega_p/\omega_0)$. Below we present simulations in which complete RBS suppression is reached for $a_0 a_1 \sim 0.1$ at $\omega_p/\omega_0 \approx 0.15$, in approximate agreement with this analytical prediction.

It is stressed that RBS suppression by RFS works for both lower ($a_0 \leqslant 1.0$) and higher ($a_0 \geqslant 1.5$) laser intensities but is only advantageous at higher intensities for the following reason. In a regime of low laser intensity, the growth of both RBS and RFS is also rather low. One consequence of this is that the laser wake (RFS Langmuir wave) may not break, so it will only accelerated electrons that are injected into it by the RBS Langmuir wave. Another consequence is that the amount of electrons injected into the wake by RBS is too low to cause considerable wake damping. Suppression of RBS in the low-intensity regime will not lead to a significantly larger wake, but will decrease the number of plasma electrons eligible for acceleration by the wake. The net result is that RBS suppression at lower laser intensities hurts fast-electron production, in agreement with earlier results [5, 14–19] and fully supported by our simulation results below.

After having established that RBS reduces the production of high-energy electrons for laser-pulse intensities well above the trapping threshold, while RFS improves it by both enhancing the laser wake and suppressing RBS, we are now ready to investigate the role of various laser and plasma parameters on both RBS and RFS growth, and the consequences of this influence for high-energy electron yield. This is done in the next section.

3. Effects of laser and plasma parameters on RBS and RFS

As known from previous research, a number of laser and plasma parameters influence the growth of RBS and/or RFS. For example, the effect of plasma inhomogeneity on RBS has been studied by Liu et al. [31]. They found that for a very long pump pulse moving up a slope in the density profile, the RBS growth rate calculated in the Wentzel Kramers Brillouin (WKB) limit decreases with increasing slope. However, this result has been derived under the assumption that the pump pulse is very long, and hence does not directly apply to RBS produced by ultrashort pulses. The effect of asymmetric pulse envelopes on RBS has been studied by Coverdale et al. [32], who showed that an asymmetric pulse leads to an asymmetric frequency spectrum, thus shifting the balance between RBS and RFS growth.

A parameter that recently received a lot of attention as a means for controlling both the growth of Raman instabilities and the yield of high-energy electrons is laser chirp, i.e. change of carrier frequency through the laser pulse. The chirp is called *positive* if the carrier frequency increases from front to back, and *negative* otherwise. In experiments, chirp is usually introduced by detuning the double-pass

https://doi.org/10.1017/S0022377804003320 Published online by Cambridge University Press

compressor grating in the chirped pulse amplification process [33]. The influence of laser chirp on RBS growth has been studied analytically by Sakharov and Kirsanov [23], and both analytically and experimentally by Faure et al. [34]. Both investigations yielded that the RBS growth depends on the magnitude, but not the sign, of the chirp. In addition, Sakharov and Kirsanov found that RBS is suppressed by the chirp if $\omega_0^{-1}|\partial\omega_0/\partial x| > \frac{1}{2}(\omega_p/(c\sqrt{\gamma_0}))(a_0^2/\gamma_0^2)$, where $\partial\omega_0/\partial t = -(\omega_0/k_0)\partial\omega_0/\partial x$ represents the chirp, $\gamma_0 = \sqrt{1+a_0^2}$, and the laser pulse propagates in the x-direction. The influence of chirp on RFS has also been investigated by Mori [35] and Schroeder et al. [36]. In both cases it has been found that a positive (negative) chirp enhances (reduces) RFS growth. At this point, it should be stressed that the effect of chirp on both RBS and RFS depends on the quantity $\partial\omega_0/\partial x$, rather than on the relative frequency change $\delta\omega/\omega_0$ along the whole pulse length.

Starting from an unchirped pulse with a given length and bandwidth, linear laser chirp can be applied in essentially two ways: pulse-length preserving and bandwidth preserving. If the pulse length is preserved, then the fast phase ψ at $x = 0$ of the laser EM wave is given by $\psi(t) = \omega_0 t + at^2/(2t_p^2)$, where t_p denotes the root-mean-square duration of the pulse. It then follows that the bandwidth of the pulse increases by a factor $\sqrt{1+a^2}$. If the bandwidth is preserved, then ψ at $x = 0$ is given by $\psi(t) = \omega_0 t + (a/(1+a^2))t^2/(2t_p^2)$. This causes the pulse duration to increase by a factor $\sqrt{1+a^2}$. Confusingly, the quantity a/t_p^2 is often referred to as 'chirp' in *both* cases. If we compare the gradient of the carrier frequency for both cases, we find that $\partial\omega/\partial t = \partial^2\psi/\partial t^2 = a/t_p^2$ for pulse-length-preserving chirp, while this rate equals $(a/(1+a^2))/t_p^2$ for bandwidth-preserving chirp. This means that in the first case, the gradient can reach arbitrarily large values, while in the second case, the rate reaches its maximum (minimum) value of $\pm 1/(2t_p^2)$ for $a = \pm 1$, and quickly drops off to zero for $|a| > 1$. For a more detailed discussion on laser chirp, see, for example, Malinovsky and Krause [37].

Since the two types of chirp have such different characteristics, they can also be expected to have very different effects on RBS and RFS growth. Pulse-length-preserving chirp is characterized by a large value for $\partial\omega_0/\partial x$, which leads to a significant reduction or even total suppression of RBS growth and a marked increase (decrease) of RFS growth for positive (negative) chirp. Bandwidth-preserving chirp on the other hand displays only a small value for $\partial\omega_0/\partial x$ and is mainly characterized by pulse length increase, especially for large $|a|$. Due to the longer pulse–plasma interaction length, this results in a much increased level of RBS growth for this type of chirp, regardless of sign. This effect dwarfs any effect of the carrier frequency gradient, and as a result, the main effect of bandwidth-preserving chirp is an increase in RBS growth independent of the sign of the chirp.

We wish to stress the point that in experiments, a laser pulse is virtually always chirped by passing it through an appropriate set of dispersive optics, so its power spectrum and thus its bandwidth are more or less preserved. This way, chirping a pulse is more a method to increase the pulse length than a method to induce a carrier frequency gradient inside the pulse. As a consequence, this gradient is nearly always small for chirped pulses in experimental situations.

The effect of chirp on fast-electron yield is as follows. Since pulse-length-preserving chirp suppresses RBS, its effect on fast-electron yield relies completely on its effect on RFS. Therefore, a positive (negative) chirp of this type is predicted to enhance (reduce) fast-electron yield. The predicted effects on both RFS and fast-electron yield have been observed in simulations by Dodd and Umstadter [38]

focusing on the effects of this type of chirp. Bandwidth-preserving chirp on the other hand has an entirely different influence on fast-electron yield. As the sign of this type of chirp hardly has an effect on either RBS or RFS, it is not expected to influence fast-electron yield either. Initial experiments on the dependence of electron yield on the chirp of a short laser pulse indicated that more electrons were produced for positively than for negatively chirped pulses [11]. However, in a recent paper by Leemans et al. [7] the origin for this effect in their experiments was shown to be important pulse shape changes that accompanied changes in the frequency chirp. Due to higher-order dispersion in the optical components of the chirped-pulse amplification (CPA) laser system, a change in the grating separation distance resulted in a change in the pulse duration, amplitude, frequency chirp, as well as the temporal profile (skew) of the laser pulse, such that the pulse bandwidth and energy remained approximately constant. Measurements of the pulse shapes using a frequency resolved optical gating (FROG) system [39] revealed that the positively (negatively) chirped pulse had a fast (slow) rise time and a slow (fast) fall time [40]. As discussed later, the effect of the fast rise time was to enhance the RFS growth, resulting in larger electron yields. Recently, they have succeeded in decoupling the chirp and the pulse shape modifications, and have subsequently produced pulses with negative (positive) chirp and fast (slow) rise time, and shown that again, the electron yield peaks for pulses with fast rise time, independent of the sign of the chirp.

In conclusion, the following can be said about the effect of chirp on fast-electron yield. Pulse-length-preserving chirp does have a significant effect on fast-electron yield, but this type of chirp is usually not used in experiments. Therefore, the claims by Dodd and Umstadter [38] (who used pulse-length-preserving chirp) that their results are in agreement with experiments are unfounded. Furthermore, they assumed a laser chirp corresponding to a relative full width at half maximum (FWHM) bandwidth $\Delta\omega/\omega_0$ of approximately 24%, which is nearly an order of magnitude beyond that used in typical experiments. On the other hand, bandwidth-preserving chirp as used in experiments does not either significantly suppress RBS or significantly influence RFS. Its only important effect is an increase of RBS, and thus a decrease of fast-electron yield, with the magnitude of the chirp. All in all, chirping a laser pulse should not be expected to increase fast-electron yield in experiments.

In the next section, simulation results are presented that focus on the connection between the influence of a parameter on RBS or RFS growth for laser intensities well beyond the electron trapping threshold, and the influence of that parameter on energetic electron production. We have investigated the effects of plasma density profile, pulse envelope modification, and both bandwidth- and pulse-length-preserving chirp. In each case, we show that if a parameter increases RFS and/or decreases RBS, this will increase the electron yield, while if a parameter decreases RFS and/or increases RBS, this will decrease the electron yield.

4. Simulations

This section is organized as follows. First, the setup of our simulations is explained. In the next two sections, the respective roles of RBS and RFS in the production of high-energy electrons for higher pulse intensities are investigated. In the case of RFS, we concentrate mostly on its role in the suppression of RBS, since its role

https://doi.org/10.1017/S0022377804003320 Published online by Cambridge University Press

in enhancing the wakefield is already well known [24, 30]. In the remainder of this section, the effect of plasma density profile, laser envelope shape and laser chirp (both pulse-length- and bandwidth-preserving chirp) on fast-electron production are investigated. It is argued that the effect of each parameter on fast-electron yield can be explained from their influence [32, 34] on the balance between RBS and RFS growth during pulse–plasma interaction. This knowledge can be used to tune those parameters such that RBS growth is minimized and fast-electron production is maximized.

4.1. Simulation setup

For our simulations, the one-dimensional version of the code XOOPIC [41] has been used. This code uses Yee's method to integrate the time-dependent Maxwell equations [42]. In the simulations, a laser pulse has been launched onto a slab of underdense plasma. The pulse propagates along the x-coordinate. For the simulations with pulse-length-preserving chirp (see below), we have used a constant plasma density $n_0 = 1.116 \times 10^{19}$ cm$^{-3} = 0.01\, n_{\rm cr}$, to match earlier simulations [38] using this type of chirp. For the other simulations, laser and plasma parameters have been chosen to match those used in experiments by Leemans et al. [7]. In those, two different plasma electron density profiles have been employed. The first is a rather flat-top profile given by $n(x) = n_0 \exp(-x^6/l^6)$ where $l = 539$ μm and $n_0 = 0.022\ n_{\rm cr} = 3.8 \times 10^{19}$ cm^{-3}. The second profile is Gaussian, $n(x) = n_0 \exp(-x^2/(2l^2))$ where $l = 530$ μm and $n_0 = 0.017\ n_{\rm cr} = 2.9 \times 10^{19}$ cm^{-3}. For both profiles, $n_{\rm cr} = \varepsilon_0 m_{\rm e} \omega_0^2 / e^2$ is the critical density for the propagation of an EM wave having carrier frequency ω_0. The ions are treated as an immobile, charge neutralizing background.

Laser pulses are brought into the simulation through a time-dependent boundary condition for the electric field at the left edge of the simulation window, and move from left to right. The laser pulse has a carrier wavelength $\lambda_0 = 800$ nm, and linear polarization with $E_z = 0$. A number of envelope shapes has been used, all derived from a standard Gaussian envelope which we will refer to as a type 0 envelope. This type of envelope is described by $E_0 \exp(-t^2/(2t_{\rm p}^2))$, where $E_0 = (m_{\rm e}\omega_0 c/e)a_0$ denotes the peak amplitude, and $t_{\rm p}$ the pulse time. The standard envelope has $t_{\rm p} = 30$ fs, so the pulse has a FWHM of 50 fs. We either use this envelope as it is, or modify it by adding bandwidth-preserving chirp, pulse-length-preserving chirp or 'skew' (non-symmetric deformation) to it. This results in the following three types of time-dependent boundary conditions, applied at a time when the left edge of the simulation window corresponds to a large negative value of x ($\Re$ denotes the real part of an expression).

(i) Chirped Gaussian pulse with constant bandwidth:

$$E_y(t) = \Re\big(E_0/\sqrt[4]{1+a^2}\exp\big[-(1+ia)t^2/\big(2(1+a^2)t_{\rm p}^2\big)\big]\exp(-i\omega_0 t)\big),$$

where a is the chirp parameter. The length of this pulse is given by $t_{\rm p}\sqrt{1+a^2}$, while its amplitude is $E_0/\sqrt[4]{1+a^2}$, such that the total energy of the pulse remains constant. The FWHM bandwidth for this pulse is $\Delta k/k_0 = 2\sqrt{2\ln(2)}/(ck_0 t_{\rm p})$.

(ii) Chirped Gaussian pulse with constant pulse length:

$$E_y(t) = \Re\big(E_0\exp\big[-(1+ia)t^2/\big(2t_{\rm p}^2\big)\big]\exp(-i\omega_0 t)\big),$$

https://doi.org/10.1017/S0022377804003320 Published online by Cambridge University Press

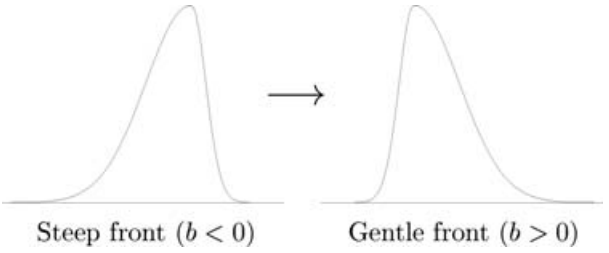

Figure 1. Sample 'skewed' pulse envelopes for negative/positive b. The arrow denotes the direction of propagation.

where a has the same definition as before. Both pulse length and amplitude are conserved as the pulse is chirped. The FWHM bandwidth for this pulse is $\Delta k/k_0 = (2\sqrt{2\ln(2)}/(ck_0t_\mathrm{p}))\sqrt{1+a^2}$.

(iii) Unchirped pulse with deviation from Gaussian envelope:

$$E_y(t) = \Re(E_0 \exp\left[-t^2/\left(t_\mathrm{p}^2\left(1 + bt/\sqrt{t_0^2 + t^2}\right)\right)\right] \exp(-i\omega_0 t)),$$

where $t_0 = 1\ \mu\mathrm{m}/c$ by definition, and b is a dimensionless parameter to control the 'skewness' of the pulse, $|b| < 1$. For $b < 0$, the pulse has a steep front and a gentle back; for $b > 0$ it is the other way around. Sample envelopes for $t_\mathrm{p} = 50$ fs and $b = \pm 0.8$ are shown in Fig. 1.

For all envelope types, a_0 takes values between 0.5 and 3.0. Other parameters are $t_\mathrm{p} = 30$ fs and $a = 0, \pm 1, \pm 5.9$ for the type (i) pulse, and $t_\mathrm{p} = 80$ fs and $a = 0, \pm 15.4$ for the type (ii) pulse (to match the pulse in [38]). For the type (iii) pulses used in [7], one has $t_\mathrm{p} = 50$ fs, $b = -0.52$ for the steep-front pulse and $t_\mathrm{p} = 52$ fs, $b = 0.58$ for the gentle front pulse. For $a = 0$ ($b = 0$) all envelope shapes reduce to the standard type 0 (Gaussian) envelope.

One should note that the total energy in a type (iii) pulse varies with b as $(1 - 0.12b^2)$, whereas the total energy in type (i) or (ii) pulses is independent of a. However, for $b = 0.58$ (-0.52), the pulse energy is only 4.5% (3.5%) lower than for $b = 0$, so the differences are well within the accuracy of the values for a_0 as taken from the experiments.

A moving window has been used to follow the pulse. The simulation has been continued for either 5.33 or 12 ps depending on the width of the plasma slab, to allow the pulse to completely traverse the plasma. A simulation box of 0.2 mm with 5120 cells has been used (cell size 39 nm, i.e. 20–25 cells per laser wavelength), and 32 particles per cell at peak density. At the boundaries, absorbing boundary conditions have been applied, so no reflected radiation will interfere with the simulation.

The numerical removal of all left-going, i.e. backward-going, radiation mentioned above has been implemented as follows. In one dimension, the transverse EM fields can be separated into left-going ($\mathbf{E}_\mathrm{l}, \mathbf{B}_\mathrm{l}$) and right-going ($\mathbf{E}_\mathrm{r}, \mathbf{B}_\mathrm{r}$) parts, provided the plasma density changes on a length scale much longer than the laser or plasma wavelength. One then has $\mathbf{E}_\perp = \mathbf{E}_\mathrm{l} + \mathbf{E}_\mathrm{r}$ and $\mathbf{B}_\perp = \mathbf{B}_\mathrm{l} + \mathbf{B}_\mathrm{r}$, where $\mathbf{E}_l = \frac{1}{2}(0, E_y - cB_z, E_z + cB_y)$, $\mathbf{E}_\mathrm{r} = \frac{1}{2}(0, E_y + cB_z, E_z - cB_y)$, $\mathbf{B}_\mathrm{l} = \frac{1}{2}(0, B_y + E_z/c, B_z - E_y/c)$ and $\mathbf{B}_\mathrm{r} = \frac{1}{2}(0, B_y - E_z/c, B_z + E_y/c)$. This separation is accurate up to $\mathbf{O}(\omega_\mathrm{p}^2/\omega_0^2)$,

https://doi.org/10.1017/S0022377804003320 Published online by Cambridge University Press

which is sufficient to achieve a near-complete RBS suppression while leaving the right-going fields virtually unaffected. In those simulations where field suppression has been used, the transverse EM fields have been replaced by their right-going parts once every 100 time steps during the first 2 ps. After 2 ps, field suppression has been discontinued since RBS is negligible at that stage and continuation of the suppression may eventually affect the right-going fields. This is because the transverse components of **E** and **B** are known at different points of the Yee mesh [42] and have to be interpolated for the calculation of the right-going fields, which introduces numerical errors.

Absent in our simulations are two-dimensional effects such as Raman sidescatter, self-focusing, and direct laser acceleration [43], which could play an important role in certain regimes. However, both RBS and RFS are basically one-dimensional instabilities that can be studied using one-dimensional simulations. Moreover, the simulations presented by Mori et al. [22] demonstrated that also in two dimensions the presence of RBS and RSS causes large amounts of slow electrons to be injected into the wakefield, loading the wakefield and reducing its amplitude. Finally, it is noted that the longitudinal electric field of a particle in one dimension does not depend on its Lorentz factor γ, whereas this field scales with $1/\gamma^2$ in three dimensions due to relativistic effects. As long as the density of trapped electrons is much lower than the plasma electron density, this does not make a difference to the longitudinal beam loading of a trapped electron [44]. However, in the case that the density of trapped electrons is much higher than that of the plasma electrons, the γ-dependence of the longitudinal electric field induces a clear γ-dependence of the longitudinal beam loading in three dimensions, which cannot be reproduced in one dimension. For the parameters used in our simulations, the γ-dependence of the beam loading will be in between these two extremes. However, the simulation results will show that the wake damping is mainly caused by slow particles ($\gamma^2 < 1.3$), for which the longitudinal beam loading in one dimension is not very different from three dimensions. Therefore, this issue does not affect the validity of our results.

Several benchmarks have been performed to establish the reliability of the code XOOPIC. In the weakly nonlinear regime $a_0 \leqslant 1$, both the laser pulse and the scattered EM waves have to satisfy the dispersion relation $\omega^2 - \Omega_p^2 = c^2k^2$, where $\Omega_p^2 = \omega_p^2/\sqrt{1 + a_0^2}$ is the relativistically corrected plasma frequency. Furthermore, the backscattered wave needs to satisfy $|\omega_- - \omega_0| = \Omega_p$ and $|k_- - k_0| = \Omega_p/c$. The RBS Langmuir wave needs to satisfy $\omega = \Omega_p$ and $k = 2k_0 - \Omega_p$. A simulation involving a pulse with $a_0 = 0.5$ and a plasma $n_0 = 3.8 \times 10^{19}$ cm^{-3} has been performed, and the results satisfy all of the above relations within accuracy limits.

We have also performed benchmarks to reproduce results on RFS stimulation in beat-wave experiments [24], RFS stimulation through direct RFS seeding [30], and suppression of RBS by RFS in beat-wave experiments [28, 29], all obtained in the linear regime. Simulations have been performed with $a_0 = 0.2$ for the RFS seeding case and $a_0 = 0.1$ for both pulses in the beat-wave case. The effects described in the papers mentioned have all been reproduced. Therefore, we consider the code to be sufficiently reliable for our needs.

4.2. Effect of RBS

As explained in Sec. 2, in the regime of high laser intensities the presence of RBS is expected to decrease the number of generated high-energy electrons, while its

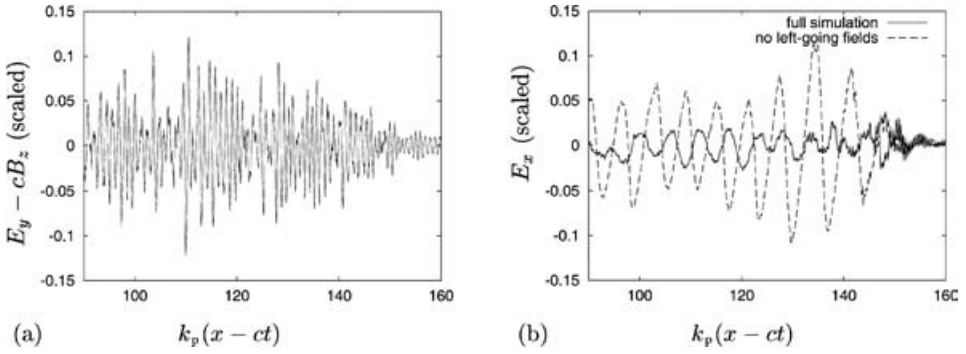

Figure 2. Simulation results for $a_0 = 1.5$ at $t = 1.6$ ps. The pulse is located between $k_p(x - ct) = 120$ and 180. (a) Left- (i.e. backward-)going transverse electric field for a full simulation. (b) Longitudinal electric (wake) field (RFS Langmuir wave) for a full simulation (solid curve) and one with suppression of left-going fields (dashed curve). In the full simulation, RBS and RFS overlap in space and time. Absence of RBS-induced beam loading in the other simulation leads to a higher amplitude wake field.

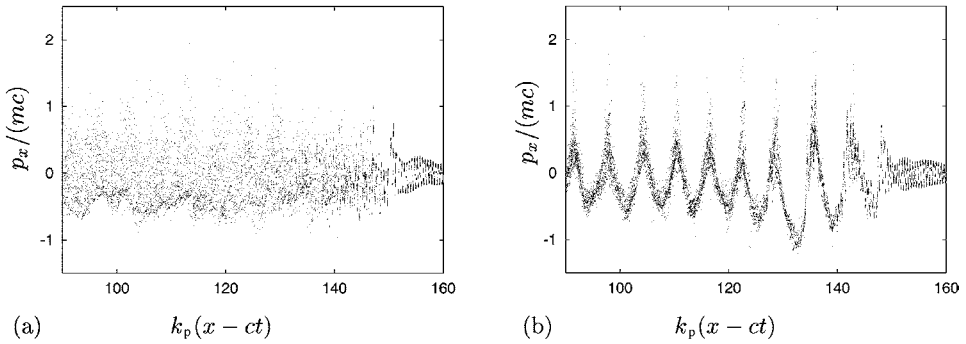

Figure 3. Simulation results for $a_0 = 1.5$ at $t = 1.6$ ps. Particle phase space for (a) a full simulation and (b) one with suppression of left-going fields. Absence of RBS-induced beam loading in the latter leads to a clearer structure in phase space, which is also related to the clearer wakefield structure visible in Fig. 2(b).

suppression is predicted to improve fast-electron production. In order to isolate the effect of RBS suppression on the number of high-energy particles we have performed two simulations for a type 0 pulse having amplitude $a_0 = 1.5$, one full simulation and one with suppression of left-going fields, as described above. The amplitude has been chosen such that the nonlinear RBS growth rate is maximum, while the nonlinear RFS growth rate is only slightly below its maximum [23]. The laser pulse has a FWHM of 50 fs, and the plasma has the flat-top density profile described above with $n_0 = 3.8 \times 10^{19}$ cm^{-3}. The results are displayed in Figs 2 and 3. In both figures, the laser pulse is located roughly between $k_p(x - ct) = 120$ and 180. Simulation results are as follows. Figure 2 displays plots of the transverse left-going field $E_{l,y}$ for the full simulation and the wake electric field E_x for both simulations, at $t = 1.6$ ps, i.e. when the pulse is in a region of increasing plasma density and the RBS growth is at its peak. The corresponding detail plots of electron phase space are displayed in Fig. 3. The plots of $E_{l,y}$ and E_x, show that RBS and RFS are both

https://doi.org/10.1017/S0022377804003320 Published online by Cambridge University Press

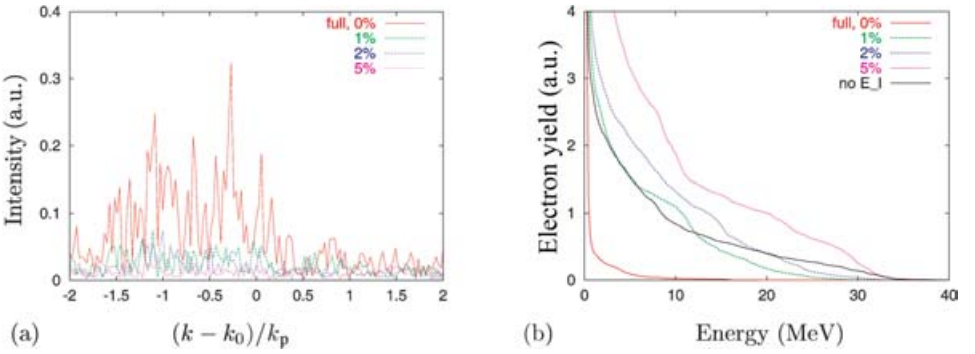

Figure 4. Simulation results for $a_0 = 1.5$, and a Stokes satellite of 0, 1, 2 and 5%, at $t = 2$ ps. (a) Fourier spectrum of the left-going transverse electric field, showing the decrease in RBS. (b) Cumulative particle energy spectra, showing the increase in high-energy particle yield. The curves labelled 'full' and 'no E_l' correspond to the same simulations as displayed in Fig. 2 and 3.

present in the simulation at $t = 1.6$ ps, and overlap in space and time, making the RBS–RFS two stage acceleration possible. The laser wake visible in the plot of E_x (Fig. 2(b)) is actually the RFS Langmuir wave. Ponderomotive excitation does not play a role here since the pulse length is several times the plasma wavelength. The plot of E_x clearly shows that the suppression of RBS in a simulation leads to a much higher wakefield amplitude, in agreement with our earlier prediction.

The phase space plots (Fig. 3) indicate that RBS-induced plasma heating is dominant in the full simulation, meaning that a large number of particles is available to be trapped by the wake wave. As a result, the laser wake is heavily beamloaded and has hardly any structure. In contrast, plasma heating is much less important in the simulation with suppression of left-going fields, and the laser wake has a well-defined structure, confirming our earlier speculation. It was also found that the peaks in phase space, which consist of electrons trapped in the wake, extend to much higher momenta for the simulation with suppression than for the full simulation (not shown in the phase space plots). This too points to a higher wake amplitude at wave breaking.

For both simulations particle energy spectra have been determined at $t = 2$ ps when the pulse enters the 'plateau' of maximum plasma density and the amount of trapped particles begins to saturate, and at $t = 4$ ps when the pulse leaves this plateau. At 2 ps it has been found that the simulation with suppression of left-going fields contains about 15 times as many electrons having an energy of 5 MeV or more than the full simulation. Also, the simulation with suppression displays a peak particle energy of 38 MeV, compared with 19 MeV for the full simulation. Cumulative electron energy spectra are displayed in Fig. 4(b). The simulation with suppression is labelled 'no E_l'. At later times, the particle energies have increased for both simulations, especially for the full simulation. Nevertheless, the simulation without left-going fields shows 50% more electrons having an energy above 5 MeV and six times as many electrons having an energy above 25 MeV than the full simulation. At lower laser intensities, the regime under consideration is lost. At $a_0 = 1.0$ and for the given plasma density, simulation results show that RBS growth is limited and there is little RBS-induced heating. As a result, few particles are trapped by the wake even though RBS and RFS overlapped in space, and the

https://doi.org/10.1017/S0022377804003320 Published online by Cambridge University Press

effect of beam loading of the wake can be neglected. Therefore, the suppression of RBS will not lead to a larger wake amplitude but only result in a lower fast-particle yield, in line with earlier results [5, 14–19].

Although the direct removal of all left-going fields is a useful tool for demonstrating the effect of RBS on high-energy electron yield, RBS suppression in experiments needs to be achieved in other ways. One way, as presented in the previous section, is stimulation of RFS in laser–plasma interaction. This can be achieved by simultaneously injecting two laser pulses having carrier frequencies that differ by ω_p into the plasma [24, 30]. This method will be investigated in the next section.

4.3. Effect of RFS

In the second series of simulations, the effects of RFS on plasma wave formation and fast-particle production have been investigated. Initially, the laser pulse beats with the RFS-associated Langmuir wave (ω_p, k_p), to produce Stokes and anti-Stokes sidebands at $\omega_\pm = \omega_0 \pm \omega_p$ in the Fourier spectrum of the forward-going transverse fields, which are commonly used to identify RFS [2, 27]. In turn, the beating between these side bands and the laser pulse resonantly drives the plasma wave, since their frequency difference is ω_p, driving it to much higher amplitudes than can be expected from ponderomotive excitation alone [18, 19, 24]. This is accompanied by the excitation of higher-order (anti-)Stokes EM waves, i.e. resonance peaks at $\omega_n = \omega_0 + n\omega_p$, n integer. As the sidebands gain intensity, their mutual nonlinear interaction causes sidebands at non-integer values of n to appear. This process eventually leads to the breakup of the spectrum and the laser pulse.

In order to investigate the effects of RFS more closely, simulations have been performed in which RFS has been stimulated by adding a Stokes satellite pulse to the main laser pulse, a small pulse with frequency $\omega_1 = \omega_0 - \omega_p$ and the same length and envelope shape as the main pulse. Such a satellite is expected to enhance the effect of RFS in terms of sideband growth and plasma wave excitation [24, 30]. The RFS stimulation is best observed at $a_0 \sim 0.5$, since nonlinear interaction occurring for larger a_0 quickly obscures the emergence of (anti-)Stokes peaks in the field spectra. Two simulations have been performed, one with a pulse with $a_0 = 0.5$ and a seed with $a_1 = 0.05$, and one without seed and a pulse with $a_0 = 0.55$, so the peak amplitudes are initially equal. The simulations have been continued for 5.33 ps, allowing the pulse to complete its transition through the plasma slab.

Since the effect of RFS seeding on (anti-)Stokes sideband growth and RFS Langmuir wave excitation has already been investigated in detail [30], we just summarize our results on those topics here. In both simulations, the following chain of events can be observed: emergence of the lowest order (anti-)Stokes peaks in the spectrum and of the RFS Langmuir wave behind the pulse, emergence of higher order (anti-)Stokes peaks and further growth of the Langmuir wave, energy cascading from the main laser peak to the various (anti-)Stokes peaks, emergence of non-integer (anti-)Stokes peaks due to nonlinear interaction between the various peaks, and finally loss of all structure of the transverse fields, their spectrum and the Langmuir wave as a result of this nonlinear interaction. The main difference between the two simulations is that all of these processes happen more intensely and on a much shorter timescale in the simulation with seed, than in that without.

To investigate the effect of direct RFS stimulation on RBS growth and fast-electron production, we have repeated the full simulation discussed in Sec. 4.2 with a Stokes satellite pulse added to the main laser pulse. The results are displayed in

Fig. 4. Comparing simulation results at $t = 2$ ps for $a_0 = 1.5$ and satellite levels of 0, 1, 2 and 5% of a_0, we find that the number of high-energy electrons increases with satellite amplitude (Fig. 4(b)), while RBS growth decreases (Fig. 4(a)). For the 50 fs pulse used here, a 5% satellite is sufficient to achieve near-complete RBS suppression. Simulation results indicate that a longer pulse leads to a higher RBS level, but also that this can be compensated for by using a higher seed. Therefore, we conclude that adding a Stokes satellite to the main pulse is a possible way to control the amount of RBS in laser–plasma interaction experiments. Comparing the electron energy spectra of these simulations with those of the simulation without left-going fields from Sec. 4.2 (black curve in Fig. 4(b)), we find that the simulation without left-going fields produces more high-energy particles than a full simulation with 2% seed, but less than one with 5% seed. This is explained by the fact that the seed does not only suppress RBS, but also resonantly drives the wakefield, causing a larger amplitude wakefield and therefore a larger high-energy particle yield than RBS removal alone.

Summarizing these results, we conclude that the presence of the satellite enhances the growth of RFS in the simulation, and thus the growth of the (RFS-driven) plasma wave. The RFS enhancement also leads to RBS suppression, in agreement with results by Everett et al. [28, 29], thus preventing heavy beam loading of the laser wake and leading to an even larger wake amplitude. Both effects ultimately lead to an increase in the yield of high-energy electrons, rendering the Stokes satellite a very effective, experimentally feasible way to stimulate fast-electron production.

In the following sections, we investigate how the RFS/RBS growth is affected by the plasma density profile, the pulse envelope shape and both types of laser chirp, and what the consequences are for the influence of such parameters on high-energy electron production.

4.4. Plasma density profile

The first parameter to be investigated is the plasma density profile. As mentioned above, for a long pump moving along a plasma density ramp, the RBS growth decreases with increasing slope [31]. Unfortunately, this result cannot be applied to the case of a short pulse, i.e. much shorter than the typical length scale on which the plasma density changes. In such cases, it is expected that the RBS and RFS growth rates are determined by the local plasma density itself at the location of the pulse rather than by the slope of the density profile at that location. The total growth is then obtained by integrating the growth rate along the profile.

To investigate the influence of the plasma density profile on both RBS/RFS growth and fast-electron production, we have performed two simulations in which the same laser pulse (50 fs duration, $a_0 = 1.5$) impinges upon a plasma having a piecewise linear density profile that ramps up from $n = 0$ to 3.8×10^{19} cm^{-3} and then remains at that density. In the first simulation the ramp occurs over a distance of 0.6 mm, while in the second it occurs over 1.8 mm. The simulations have been continued until the pulses reached the plateau of maximum density in both cases, and particle trapping saturated.

Simulation results are displayed in Figs 5 and 6. For both simulations, the Fourier spectrum of the backward going fields has been determined just after the onset of plasma electron trapping, since at this time the influence of RBS on particle trapping is maximum. For the steep slope case, this happens just after the pulse

https://doi.org/10.1017/S0022377804003320 Published online by Cambridge University Press

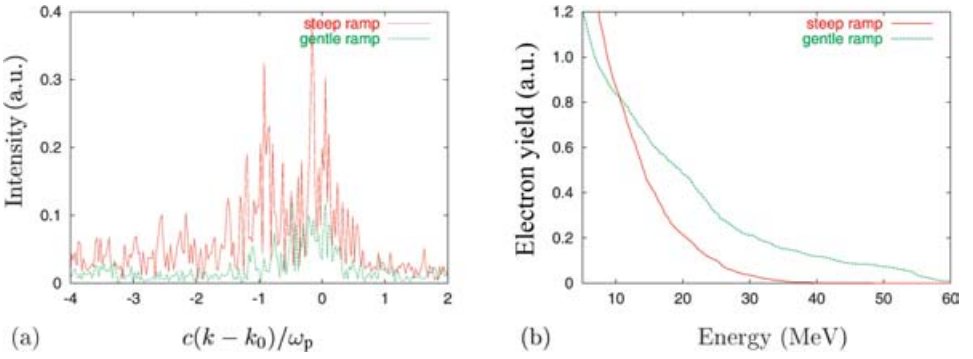

Figure 5. Fourier spectrum of the transverse electric field (a) and electron energy spectrum (b) for a plasma density profile with a steep ramp (red) and a gentle ramp (green). The gentle ramp case displays a higher fast-particle yield than the steep ramp case. This difference is related to the lower RBS growth for a gentle ramp.

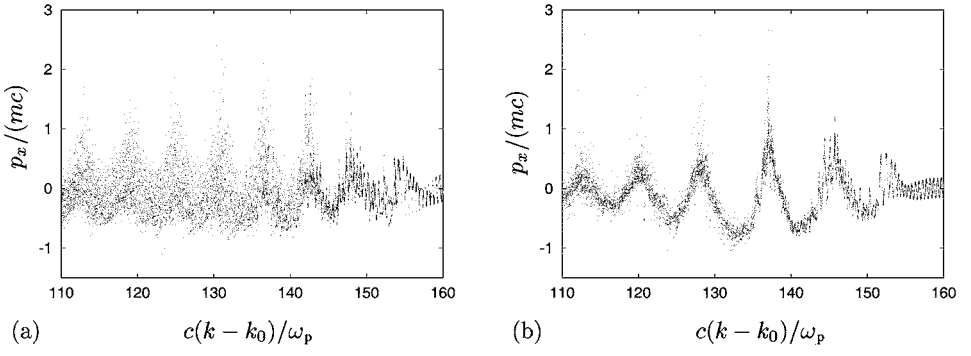

Figure 6. Detail plots of electron phase space for a plasma density profile with a steep ramp (a) and a gentle ramp (b). Phase space has more structure for a gentle ramp than for a steep ramp, and is less burdened by RBS-induced heating.

has reached maximum density ($t = 2.2$ ps), while for the gentle slope this happens when the pulse is at 65% of the maximum density ($t = 4$ ps). The spectra are shown in Fig. 5(a): it is clear that the steep slope case exhibits a lot more RBS than the gentle slope case. This is primarily due to the fact that at the onset of trapping, the pulse has reached maximum density for the steep slope case, which results in a larger local RBS growth rate. Particle energy spectra have been taken at the end of the simulations ($t = 6$ ps). They are displayed in Fig 5(b): it is obvious that once particle trapping has saturated, the pulse moving along the gentle ramp has produced much more high-energy electrons than the pulse moving along the steep ramp. It is true that the total number of trapped electrons is higher for the steep ramp case; however, nearly all of them are at the low end of the spectrum. In Fig. 6, detailed plots of electron phase space are shown for both simulations. The steep slope case clearly displays a higher level of RBS-induced plasma heating than the gentle slope case. This agrees with the above observation that there is more RBS excitation for the steep slope case than for the gentle slope case.

In general, it can be said that early in the simulations, the steep slope case displays a larger level of RBS than the gentle slope case, while the level of RFS

https://doi.org/10.1017/S0022377804003320 Published online by Cambridge University Press

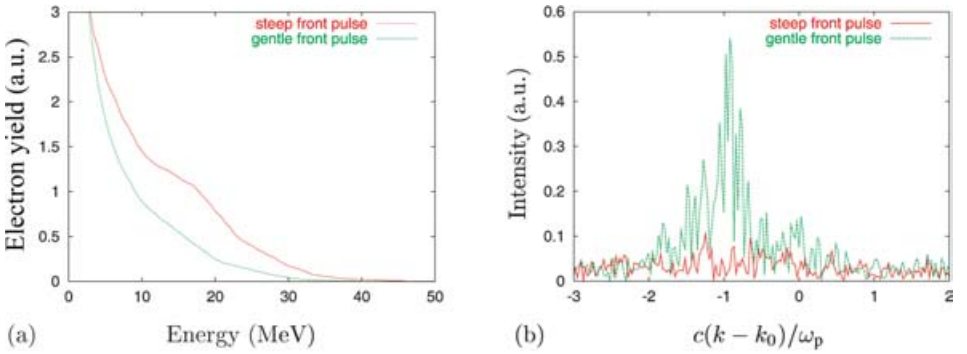

Figure 7. Particle energy spectrum (a) and Fourier k-spectrum of $E_{l,y}$ (b) for a pulse with a steep (red) and a gentle (green) front ($a_0 = 2.6$), at $t = 2$ ps. The steep front pulse generates less RBS and more high-energy particles than the gentle front pulse.

is low for both cases due to the small RFS growth rate. Later in the simulations, when RFS becomes dominant and RBS has mostly disappeared, the steep slope case exhibits a higher level of RFS than the gentle slope case. The fact that the growth rates for both RBS and RFS increase with increasing plasma density may explain this: for any x between 0 and 1.8 mm, the steep slope profile has a higher local density than the gentle slope profile. Next to that, the 'history' of the pulse, i.e. the profile already traversed before arriving at a certain density, is probably also important. The larger amount of highly energetic electrons seen in the gentle slope case is probably due to the fact that in both simulations, electron capture happens when RBS is still dominant. Consequently, the highest electron energy is reached in the simulation that exhibits the lowest RBS level. The difference in RFS at later times, which should work in favour of the steep slope case, seems to be much less important.

4.5. Laser pulse envelope

As found in experiments by Leemans et al. [7], the use of laser pulses with a 'skew' envelope influences the yield of high-energy electrons. Experimental results presented in this paper show that a pulse with a steep front and gentle back traps more electrons than one with a gentle front and steep back. Simulations have been performed using the type (iii) laser pulse envelopes given in Sec. 4.1. Pulse parameters have been chosen to match those obtained in the experiments: $t_p = 50$ fs, $b = -0.52$ for the steep front pulse, and $t_p = 52$ fs, $b = 0.58$ for the gentle front pulse. Pulse amplitude is $a_0 = 2.6$ for both simulations. The plasma density profile is the flat-top profile from Sec. 4.1. Simulation results are as follows. Figure 7 displays the cumulative electron energy spectra (a) and the Fourier spectra for the backward-going EM fields (b), both taken at $t = 2$ ps. From the energy spectra, we find that the steep front pulse generates more high-energy electrons than the gentle front pulse. The Fourier spectra reveal that the steep front pulse generates less RBS than the gentle front pulse. Figure 8 displays detail plots of the electron phase space at $t = 2$ ps, for a steep front pulse (a) and a gentle front pulse (b). It is clear from these plots that there is less RBS-induced plasma heating for a steep front pulse.

https://doi.org/10.1017/S0022377804003320 Published online by Cambridge University Press

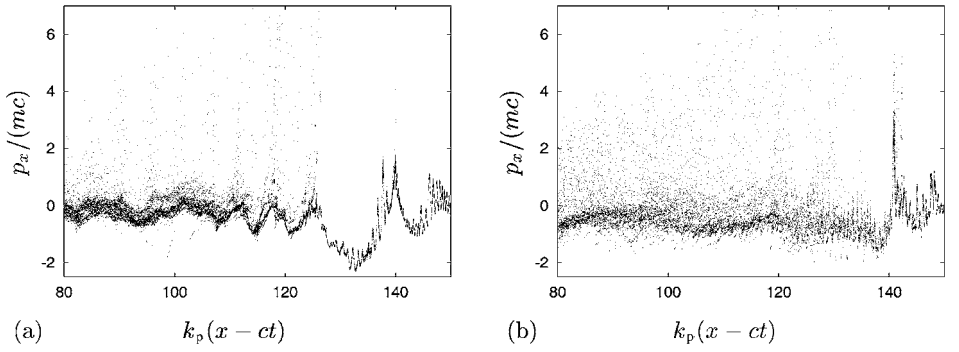

Figure 8. Detail plots of particle phase space for a pulse with a steep front (a) and a gentle front (b), for $a_0 = 2.6$ at $t = 2$ ps. The plot for the steep front pulse clearly exhibits more structure and less electron heating than that for the gentle front pulse.

The role of RFS in this case cannot readily be deduced from the simulation results. This is due to the high peak intensity of the pulses, which is well in the nonlinear regime. As a result, the (anti-)Stokes peaks of RFS do not emerge clearly from the Fourier k-spectra of the forward going EM fields, and cannot be studied. However, a linear analysis by Schroeder et al. [36] predicted that the steep front pulse causes a larger RFS growth than the gentle front pulse. This is supported by simulation results at low laser intensity by Fisher and Tajima [30] that indicated that a sharp leading pulse edge indeed favours RFS excitation. As a result, the steep front pulse excites a larger wake than the gentle front pulse, which also contributes to an increased fast-electron yield.

Based on our simulation results and the theory presented in Secs 2 and 4.2, we propose the following scheme for the effect of pulse envelope shape on energetic electron yield: (i) a steep front pulse favours RFS growth, while a gentle front pulse does the opposite; (ii) enhanced RFS growth leads to both a larger laser wake and suppression of RBS; (iii) RBS suppression leads to less beam loading of the wake and thus to an even larger wake; (iv) the combined effect of all this is a marked increase in high-energy electrons for the steep front pulse as compared with the gentle front pulse, in agreement with experimental results [7].

4.6. Pulse-length-preserving chirp

As shown by Dodd and Umstadter [38], pulse-length-preserving laser chirp has a clear effect on both RFS growth and fast-electron production. This type of chirp is characterized by its large carrier frequency gradient. In this section the effect of this type of chirp on both RBS and RFS is investigated, in order to determine whether RBS also plays a role in this case.

Several simulations with pulse-length-preserving chirp have been performed. For the plasma, $n_0 = 1.1 \times 10^{19}$ cm^{-3} has been used, and either a constant density or a flat-top plasma slab as specified above. A type (ii) pulse envelope has been used with $a_0 = 1.0$, $\lambda_0 = 1$ μm, 80 fs FWHM, and a chirp factor $a = \pm 15.4$. Simulation results are displayed in Figs 9–11. First, the pulse with positive chirp displays a lot of erosion at the front (Fig. 9(a)), where its frequency is low, while this effect is entirely absent for the negatively chirped pulse (Fig. 9(b)). This is probably caused by the fact that the vector potential $\mathbf{A}_\perp = \int \mathbf{E}_\perp \, dt$ of the pulse has an

https://doi.org/10.1017/S0022377804003320 Published online by Cambridge University Press

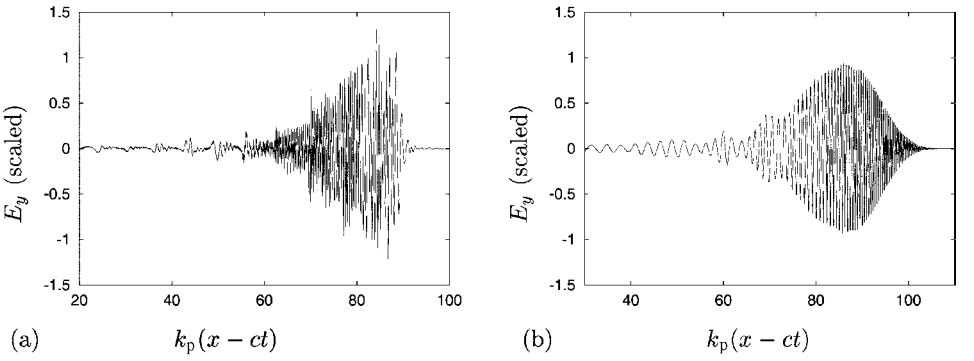

Figure 9. Transverse electric field at $t = 6$ ps for pulses with pulse-length-preserving chirp: (a) positive chirp, and (b) negative chirp. The pulse with positive chirp undergoes strong depletion at its front, while the pulse with negative chirp is hardly affected. In both cases, complete RBS suppression can be observed.

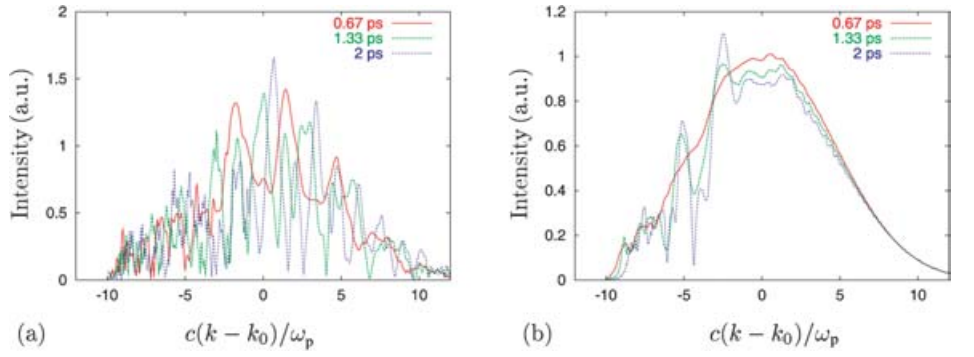

Figure 10. Fourier spectrum of transverse electric field for pulses with length-preserving chirp: (a) positive chirp and (b) negative chirp. The spectra for positive chirp display a large RFS growth, while there is hardly a trace of RFS for negative chirp.

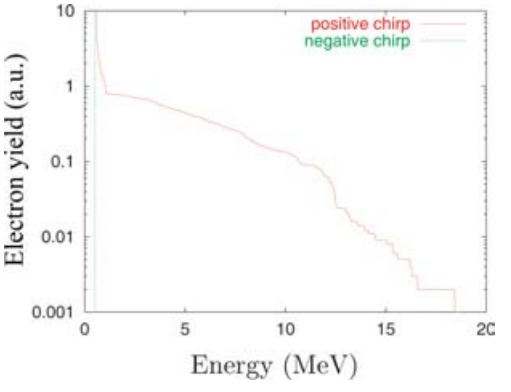

Figure 11. Electron energy spectrum at $t = 6$ ps for pulses with positive (red) and negative (green) pulse-length-preserving chirp. It is clear that positive chirp enhances fast electron yield, while negative chirp suppresses it.

https://doi.org/10.1017/S0022377804003320 Published online by Cambridge University Press

asymmetric envelope as a result of the non-constant carrier frequency of the pulse, even though the electric field has a symmetric envelope. For a positive (negative) chirp, the vector potential envelope will have a steep front (back) and a gentle back (front), which increases (decreases) RFS seeding, as the ponderomotive force of the pulse is proportional to $\nabla A_\perp^2$. (See also the previous section on the effect of asymmetric pulse envelopes.) Apart from enhancing the differences in the growth of RFS already present due to the large carrier frequency gradient (see below), the asymmetry of the vector potential is also held responsible for the asymmetric erosion of the laser pulse.

One should note that the carrier frequency gradient needs to be quite large in order to see a reasonable skewness in the envelope of **A**. This can be quantified as follows. As the local carrier frequency $\omega(t)$ of a chirped pulse depends linearly on the time t, there is a time t_0 such that $\omega(t_0) = 0$. If the chirp of the pulse is such that $|t_0| \leqslant 3 \cdot t_\mathrm{p}$, then the envelope is visibly skewed. For the chirped pulses used in this section, $|t_0|/t_\mathrm{p} \approx 2.3$ holds and the envelopes of their vector potentials are clearly asymmetric. In addition, observe that the pulses have a very broad frequency spectrum, ranging from zero to about $2\omega_0$, where ω_0 denotes the central frequency of the pulse. This means that the group velocity within the pulse ranges from about c for the highest frequencies all the way down to zero for the lowest. For a positively (negatively) chirped pulse, having the lowest (highest) frequency at the front, this may cause compression (stretching) of the pulse, in addition to the asymmetry already present in the vector potential.

Second, the pulse with positive chirp undergoes the type of breakup of its field and spectrum that points to a large RFS growth (Fig. 10(a)). This effect is again absent in the case of a negatively chirped pulse (Fig. 10(b)). The difference in RFS growth can be explained directly from the known effect of (the sign of) a large carrier frequency gradient on the RFS growth rate as discussed in Sec. 3. As a consequence, the positively chirped pulse excites a large-amplitude plasma wave, which is able to trap electrons even at the moderate peak amplitude used here. No electron trapping is to be observed in the case of a negatively chirped pulse. The ability of positively chirped pulses to trap and subsequently accelerate electrons in their wake much more efficiently than negatively chirped pulses can do is also manifested in Fig. 11. Here we have plotted the energy spectrum of electrons that are accelerated by a positively chirped pulse (red curve) and by a negatively chirped pulse (green curve). Obviously, positive chirp enhances fast-electron yield, while negative chirp suppresses it.

As can be seen in Fig. 9, there is hardly any RBS to be observed for either positive or negative chirp, something that is accompanied by a total absence of any RBS-induced plasma heating. This is in agreement with the prediction by Sakharov and Kirsanov [23], that RBS will be suppressed if the gradient of the carrier frequency is sufficiently large, regardless of its sign. The absence of RBS allows us to study the effect of RFS on the plasma wave growth, without being bothered by the disturbing effects of RBS.

4.7. Bandwidth-preserving chirp

The last parameter to be discussed is bandwidth-preserving laser chirp. For this type of chirp, the Fourier power spectrum is conserved, causing the pulse duration to increase and the amplitude to decrease with chirp. As discussed in Sec. 3, the dominant characteristic of this type of chirp is the increase in pulse length and the

https://doi.org/10.1017/S0022377804003320 Published online by Cambridge University Press

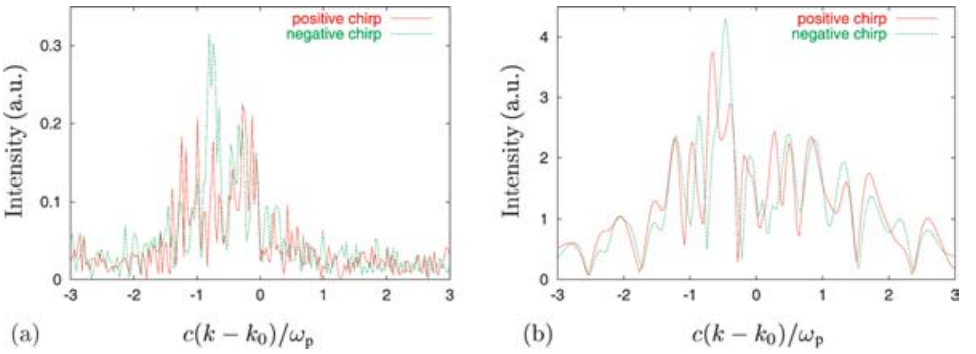

Figure 12. Fourier spectrum of the transverse electric field for pulses with small bandwidth-preserving chirp ($a = \pm 1.0$), at $t = 6$ ps, for the backward-going (a) and forward-going (b) fields. RBS growth is limited because the pulse is still very short (∼70 fs). The influence of the sign of the chirp on both RBS and RFS growth is small.

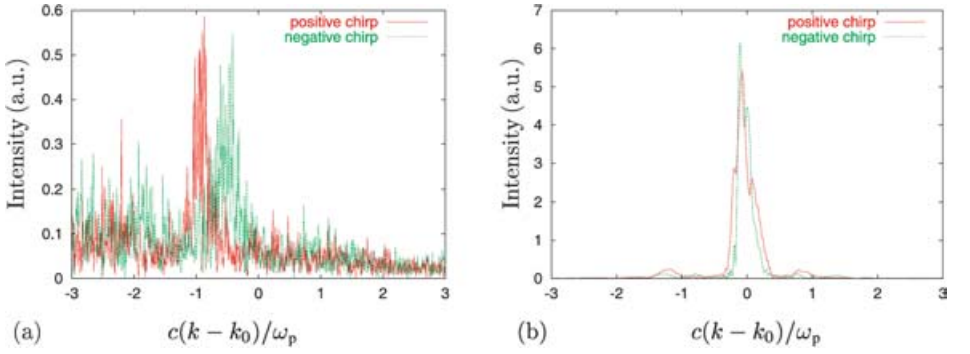

Figure 13. Fourier spectrum of the transverse electric field for pulses with large bandwidth-preserving chirp ($a = \pm 5.9$), at $t = 6$ ps, for the left-going (a) and right-going (b) fields. RBS growth is larger in this case because of increased pulse length (∼300 fs). Again, the influence of the sign of the chirp on both RBS and RFS growth is small.

corresponding decrease in amplitude, while the carrier frequency gradient is rather unimportant. Because of this, the vector potential of a pulse chirped this way is only slightly skewed, and the asymmetry in wakefield excitation mentioned in the previous section does not play a role here. Therefore, we expect the amount of RBS, and hence the particle yield, to depend on the magnitude rather than the sign of this type of chirp. To investigate this, we have performed simulations involving pulses having a type (i) envelope with $a = \pm 1.0$ and $a = \pm 5.9$. In both cases, $a_0 = 3.0$ and FWHM = 50 fs before chirping. The plasma density profile was also Gaussian, with $n_0 = 1.1 \times 10^{19}$ cm^{-3}. The following results have been obtained. In Figs 12 and 13, the Fourier spectra of the left- and right-going transverse electric field at $t = 6$ ps are shown for both small and large chirp. We see that the spectra for pulses with small chirp ($a = \pm 1.0$) are dominated by RFS in the right-going fields and show little RBS in the left-going fields, while those for large chirp ($a = \pm 5.9$) show hardly any RFS, but display a significant amount of RBS. This behaviour agrees with

https://doi.org/10.1017/S0022377804003320 Published online by Cambridge University Press

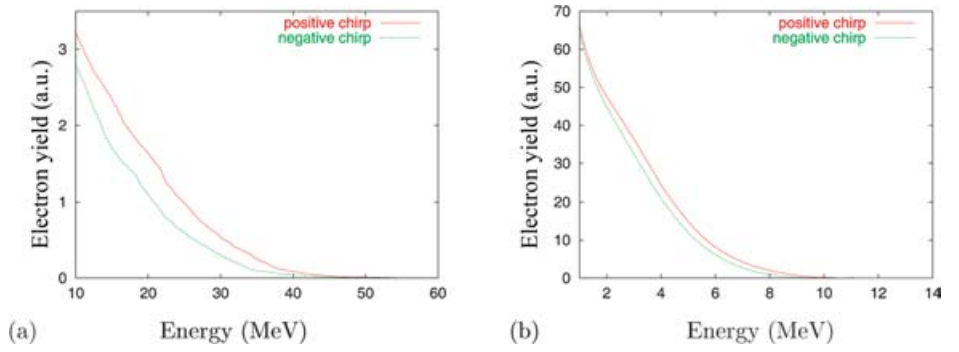

Figure 14. Cumulative particle energy spectrum for pulses with bandwidth-preserving chirp at $t = 6$ ps, for (a) $a = \pm 1.0$ and (b) $a = \pm 5.9$. The average particle energy decreases strongly with increasing chirp magnitude, while the sign of the chirp has hardly any influence.

the predictions made above for long pulses with a low carrier frequency gradient. Also, we observe that there is no qualitative change in the spectra when the sign of the chirp is changed while its magnitude is not. In Fig. 14, the corresponding cumulative particle energy spectra are displayed. It is clear from these spectra that particle numbers increase and particle energies decrease rapidly with increasing chirp magnitude, while they are nearly insensitive to its sign. This can be explained from the observations that RBS growth increases for increasing pulse length, i.e. increasing chirp magnitude, while the neither RBS nor RFS growth is affected by the sign of the bandwidth-preserving chirp. As explained before, an increase in the level of RBS rises the amount of trapped particles but strongly lowers their average energy. Also note that the number of trapped electrons naturally increases with increasing pulse–plasma interaction length.

5. Summary and conclusions

A new regime for the effect of Raman instabilities on the production of fast electrons in laser–plasma interaction has been identified. The regime is characterized by laser intensities well above the threshold for electron trapping, large growth rates of the Raman instabilities, and spatial and temporal overlap of RBS and RFS. It has been demonstrated that in this regime the presence of RBS hurts the production of fast (over 15 MeV) electrons, whereas RBS suppression enhances this production. RBS suppression can be obtained by stimulating RFS growth. An experimentally feasible way to do this, is adding a satellite pulse at the Stokes frequency to the main laser pulse. The effects of a number of pulse and plasma parameters on fast-electron production have also been investigated. It has been found that parameters that favour RFS growth and/or suppress RBS growth, ultimately lead to an increased yield of fast electrons.

In the new regime, RBS-induced plasma heating strongly increases the number of electrons that get trapped in the wake. This results in strong beam loading, which reduces the wake amplitude. Although the total number of trapped electrons increases, the number of high-energy electrons decreases in this case. Under these circumstances, suppression of RBS leads to enhanced wake wave growth, and an

https://doi.org/10.1017/S0022377804003320 Published online by Cambridge University Press

increase of both the number of fast electrons and their energy. This is in contrast to earlier results at lower laser intensities, where RBS has been found to improve fast-electron production [5, 14–19].

Adding a Stokes satellite to the main laser pulse is an efficient way to enhance fast-electron production. The satellite acts in two ways: it enhances the laser wake, and also causes RBS suppression. Depending on the circumstances, a satellite having 5% of the field amplitude (0.2% of the intensity) of the main pulse may already be sufficient to reach a near-complete suppression of RBS. This suppression has been explained from the fact that the seed enhances the growth of RFS, which in turn reduces the growth of RBS. Enhancing RFS through other means, such as tuning various laser and plasma parameters, gives similar results. In the simulations, a high yield of fast electrons is always accompanied by a high level of RFS and a low level of RBS.

The influence of various laser and plasma parameters on fast-electron yield can be explained through their influence on RFS and RBS growth. For the plasma density profile, it has been found that a pulse climbing a gentle density increase initially excites less RBS than one meeting a steep density increase. As a result, the number of high-energy electrons generated by the pulse is higher in the case of a gentle increase than that of a steep increase. Later in the simulations, the level of RFS, and thus the laser wake, is larger for a steep than for a gentle density increase. This does not seem to have a substantial influence on the final electron energy though.

The results of the simulations focusing on the effect of the shape of the pulse envelope demonstrate that an envelope with a steep front produces less RBS than an envelope with a gentle front. Although the influence of envelope shape on RFS cannot be determined from the simulations, due to the dominance of nonlinear effects at the laser intensities employed here, analytical calculations indicate that the steep front pulse excites more RFS than the gentle front pulse. Together with the fact that enhancing RFS suppresses RBS, this may well explain the difference in RBS between the pulses. The net result is a higher number of high-energy electrons produced by the steep front pulse than by the gentle front pulse, in line with experimental results [7].

The investigations on the role of chirp reveal that in order to avoid confusion, a distinction needs to be made between bandwidth-preserving chirp and pulse-length-preserving chirp. Regarding the effect of pulse-length-preserving chirp, pulses with a large chirp of this type are found to generate hardly any RBS regardless of the sign of the chirp. RFS growth, and thus fast-electron production, is different for pulses with positive or negative chirp, in agreement with earlier results [35, 36, 38]. For bandwidth-preserving chirp, the sign of this type of chirp does not have any substantial effect on RBS or RFS growth, and thus on fast-electron yield. This is in contradiction to earlier conjectures [38], but in agreement with recent experimental results [7] showing that differences in electron yield are likely to be the result of a difference in pulse envelope rather than chirp. Furthermore, RBS growth increases with the magnitude of the chirp, since the pulse length, and thus the pulse–plasma interaction region, also increases with this magnitude. This results in increased beam loading of the generated plasma wave and a drop in the yield of truly fast electrons (energy over 15 MeV). Since laser chirp as used in experiments is bandwidth preserving by nature, it is unlikely that chirping a pulse will ever increase fast-electron yield in experiments.

Acknowledgements

This work has been supported by the Centrum voor Plasmafysica en Stralingstechnologie, the US Department of Energy, Office of High Energy and Nuclear Physics, contract DE-AC-03-76SF0098, and the project Advanced Computing for 21st Century Accelerator Science and Technology. The authors acknowledge useful discussions with C. Schroeder.

References

[1] Nakajima, K. et al. 1995 *Phys. Rev. Lett.* **74**, 4428–4431.

[2] Coverdale, C. A., Darrow, C. B., Decker, C. D., Mori, W. B., Tzeng, K.-C., Marsh, K. A., Clayton, C. E. and Joshi, C. 1995 *Phys. Rev. Lett.* **74**, 4659–4662.

[3] Modena, A., Najmudin, Z., Dangor, A. E., Clayton, C. E., Marsh, K. A., Joshi, C., Malka, V., Darrow, C. B., Danson, C., Neely, D. and Walsh, F. N. 1995 *Nature* **377**, 606–608.

[4] Umstadter, D., Chen, S.-Y., Maksimchuk, A., Mourou, G. and Wagner, R. 1996 *Science* **273**, 472–475.

[5] Moore, C. I., Ting, A., Krushelnick, K., Esarey, E., Hubbard, R. F., Hafizi, B., Burris, H. R., Manka, C. and Sprangle, P. 1997 *Phys. Rev. Lett.* **79**, 3909–3912.

[6] Malka, V., Faure, J., Marquès, J. R., Amiranoff, F., Rousseau, J. P., Ranc, S., Chambaret, J. P., Najmudin, Z., Walton, B., Mora, P. and Solodov, A. 2001 *Phys. Plasmas* **8**, 2605–2688.

[7] Leemans, W. P., Catravas, P., Esarey, E., Geddes, C. G. R., Toth, C., Trines, R., Schroeder, C. B., Shadwick, B. A., van Tilborg, J. and Faure, J. 2002 *Phys. Rev. Lett.* **89**, 174802.

[8] Esarey, E., Sprangle, P., Krall, J. and Ting, A. 1996 *IEEE Trans. Plasma Sci.* **24**, 252–288.

[9] Reitsma, A., Leemans, W. P., Esarey, E., Schroeder, C. B., Kamp, L. P. J. and Schep, T. J. 2002 *Phys. Rev. ST Accel. Beams* **5**, 051302.

[10] Catravas, P., Esarey, E. and Leemans, W. P. 2002 *Phys. Plasmas* **9**, 2428–2436.

[11] Leemans, W. P., Rodgers, D., Catravas, P. E., Geddes, C. G. R., Fubiani, G., Esarey, E., Shadwick, B. A., Donahue, R. and Smith, A. 2001 *Phys. Plasmas* **8**, 2510–2516.

[12] Tabak, M., Hammer, J., Glinsky, M. E., Kruer, W. L., Wilks, S. C., Woodworth, J., Campbell, E. M., Perry, M. D. and Mason, R. J. 1994 *Phys. Plasmas* **1**, 1626–1634.

[13] Trines, R. M. G. M., Kamp, L. P. J., Schep, T. J., Leemans, W. P., Esarey, E. H. and Sluijter, F. W. 2004 *Europhys. Lett.* **66**, 492–498.

[14] Bertrand, P., Ghizzo, A., Karttunen, S. J., Pättikangas, T. J. H., Salomaa, R. R. E. and Shoucri, M. 1994 *Phys. Rev. E* **49**, 5656–5659.

[15] Bertrand, P., Ghizzo, A., Karttunen, S. J., Pättikangas, T. J. H., Salomaa, R. R. E. and Shoucri, M. 1995 *Phys. Plasmas* **2**, 3115–3129.

[16] Tzeng, K. C., Mori, W. B., and Decker, C. D. 1996 *Phys. Rev. Lett.* **76**, 3332–3335.

[17] Tzeng, K. C., Mori, W. B. and Katsouleas, T. 1999 *Phys. Plasmas* **6**, 2105–2116.

[18] Esarey, E., Hafizi, B., Hubbard, R. and Ting, A. 1998 *Phys. Rev. Lett.* **80**, 5552–5555.

[19] Esarey, E., Schroeder, C. B., Leemans, W. P. and Hafizi, B. 1999 *Phys. Plasmas* **6**, 2262–2268.

[20] Drake, J. F., Kaw, P. K., Lee, Y. C., Schmid, G., Liu, C. S. and Rosenbluth, M. N. 1974 *Phys. Fluids* **17**, 778–785.

[21] Kruer, W. L. 1988 *The Physics of Laser Plasma Interactions*. Reading, MA: Addison-Wesley.

[22] Mori, W. B., Decker, C. D., Hinkel, D. E. and Katsouleas, T. 1994 *Phys. Rev. Lett.* **72**, 1482–1485.

[23] Sakharov, A. S. and Kirsanov, V. I. 1994 *Phys. Rev.* E **49**, 3274–3282.

[24] Joshi, C., Mori, W. B., Katsouleas, T., Dawson, J. M., Kindel, J. M. and Forslund, D. W. 1984 *Nature* **311**, 525–529.

[25] Bulanov, S. V., Kirsanov, V. I. and Sakharov, A. S. 1991 *Pis'ma Zh. Éksp. Teor. Fiz.* **53**, 540–544 (*JETP Lett.* **53**, 565–569).

[26] Trines, R. M. G. M., Goloviznin, V. V., Kamp, L. P. J. and Schep, T. J. 2001 *Phys. Rev.* E **63**, 026406.

[27] Decker, C. D., Mori, W. B. and Katsouleas, T. 1994 *Phys. Rev.* E **50**, R3338–R3341.

[28] Everett, M. J., Lal, A., Clayton, C. E., Mori, W. B., Johnston, T. W. and Joshi, C. 1995 *Phys. Rev. Lett.* **74**, 2236–2239.

[29] Everett, M. J., Lal, A., Clayton, C. E., Mori, W. B., Joshi, C. and Johnston, T. W. 1996 *Phys. Plasmas* **3**, 2041–2046.

[30] Fisher, D. L. and Tajima, T. 1996 *Phys. Rev.* E **53**, 1844–1851.

[31] Liu, C. S., Rosenbluth, M. N. and White, R. B. 1974 *Phys. Fluids* **17**, 1211–1219.

[32] Coverdale, C. A., Darrow, C. B., Decker, C. D., Naumova, N. M., Esirkepov, T. Zh., Sakharov, A. S., Bulanov, S. V., Mori, W. B. and Tzeng, K. C. 1996 *Fiz. Plazmy* **22**, 685–692 (*Plasma Phys. Rep.* **22**, 617–624).

[33] Strickland, D. and Mourou, G. 1985 *Opt. Comm.* **55**, 447–449;
Strickland, D. and Mourou, G. 1985 *Opt. Comm.* **56**, 219–221.

[34] Faure, J., Marqués, J.-R., Malka, V., Amiranoff, F., Najmudin, Z., Walton, B., Rousseau, J.-P., Ranc, S., Solodov, A. and Mora, P. 2001 *Phys. Rev.* E **63**, 065401.

[35] Mori, W. B. 1997 *IEEE J. Quantum Electron.* **33**, 1942–1953.

[36] Schroeder, C. B., Esarey, E., Shadwick, B. A. and Leemans, W. P. 2003 *Phys. Plasmas* **10**, 285–295.

[37] Malinovsky, V. S. and Krause, J. L. 2001 *Phys. Rev.* A **63**, 043415.

[38] Dodd, E. S. and Umstadter, D. 2001 *Phys. Plasmas* **8**, 3531–3534.

[39] Kane, D. J. and Trebino, R. 1993 *Opt. Lett.* **18**, 823–825.

[40] Tóth, C., de Groot, J., van Tilburg, J., Geddes, C. G. R., Faure, J., Catravas, P., Schroeder, C., Shadwick, B. A., Esarey, E. and Leemans, W. 2002 *Ultrafast Phenomena XIII* (ed. Miller, R. D., Murnane, M. M., Scherer, N. F. and Wiener, A. M.). Berlin: Springer, pp. 28–30.

[41] Verboncoeur, J. P., Langdon, A. B. and Gladd, N. T. 1995 *Comput. Phys. Commun.* **87**, 199–211.
Wurtele, J. and Lee, H.-J. 2001 Private communication.

[42] Yee, K. S. 1966 *IEEE Trans. Antennas Propag.* **14**, 302–307.

[43] Gahn, C., Tsakiris, G. D., Pukhov, A., Meyer-ter-Vehn, J., Pretzler, G., Thirolf, P., Habs, D. and Witte, K. J. 1999 *Phys. Rev. Lett.* **83**, 4772–4775.

[44] Katsouleas, T., Wilks, S., Chen, P., Dawson, J. M. and Su, J. J. 1987 *Part. Accel.* **22**, 81–99.

[45] Pukhov, A. and Meyer-ter-Vehn, J. 2002 *Appl. Phys.* B **74**, 355–361.